Odour-imagery ability is linked to food craving, intake, and adiposity change in humans

Emily Perszyk, Xue Davis, Jelena Djordjevic, Marilyn Jones-Gotman, Jessica Trinh, Zach Hutelin, Maria Veldhuizen, Leonie Koban, Tor Wager, Hedy Kober, et al.

Title: Odor imagery ability is linked to food craving, intake, and adiposity change in humans

Author List: Emily E. Perszyk[1,2], Xue S. Davis[1,2], Jelena Djordjevic[3], Marilyn Jones-Gotman[3], Jessica Trinh[1,2], Zach Hutelin[1,2], Maria G. Veldhuizen[4], Leonie Koban[5], Tor D. Wager[6], Hedy Kober[2,7], Dana M. Small[1,2,3,7,8]

Affiliations:

[1] Modern Diet and Physiology Research Center, New Haven, CT 06510, USA

[2] Department of Psychiatry, Yale University School of Medicine, New Haven, CT 06511, USA

[3] Department of Neurology and Neurosurgery, Montreal Neurological Institute and Hospital, McGill University, Montreal, QC H3A 2B4, Canada

[4] Department of Anatomy, Faculty of Medicine, Mersin University, Ciftlikkoy Campus, Mersin 33343, Turkey

[5] Lyon Neuroscience Research Center (CRNL), CNRS, INSERM, University Claude Bernard Lyon 1, France

[6] Department of Psychological and Brain Sciences, Dartmouth College, Hanover, NH 03755, USA

[7] Department of Psychology, Yale University, New Haven, CT 06511, USA

[8] Department of Medicine, McGill University Health Center, Montreal, QC H4A 3J1, Canada

Correspondence: emily.perszyk@gmail.com or dana.small@mcgill.ca

INTRODUCTORY PARAGRAPH

It is well-known that food cue reactivity (FCR) is positively associated with body mass index (BMI)[1] and weight change[2], but the mechanisms underlying these relationships are incompletely understood. One prominent theory of craving posits that the elaboration of a desired substance through sensory imagery intensifies cravings, thereby promoting consumption[3]. Olfaction is integral to food perception, yet the ability to imagine odors varies widely[4]. Here we test in a basic observational study if this large variation in olfactory imagery drives FCR strength to promote adiposity in 45 adults (23 male). We define odor imagery ability as the extent to which imagining an odor interferes with the detection of a weak incongruent odor (the "interference effect"[5]). As predicted in our preregistration, the interference effect correlates with the neural decoding of imagined, but not real, odors. These perceptual and neural measures of odor imagery are in turn associated with FCR, defined by the rated craving intensity of liked foods and cue-potentiated intake. Finally, odor imagery exerts positive indirect effects on changes in BMI and body fat percentage over one year via its influences on FCR. These findings establish odor imagery as a driver of FCR that in turn confers risk for weight gain.

MAIN TEXT

Mental imagery has been proposed to play a critical role in the amplification of cravings[3], yet not all sensory modalities are similarly imaginable. The self-reported ability to imagine sights and sounds is nearly universal, whereas the ability to imagine odors varies widely[4,6,7]. We previously demonstrated that the self-reported vividness of imagined olfactory, but not visual, stimuli positively correlates with BMI[8]. These data raise the possibility that odor imagery ability confers risk for FCR and weight gain; however, evidence for the extent to which this self-report measure reflects actual odor imagery is limited[5,9]. Also unknown is whether perceptual or neural measures of odor imagery ability are related to FCR, BMI, and weight gain susceptibility (Fig. 1).

Odor imagery ability has been quantified as the extent to which imagining an odor decreases the detectability of a weak incongruent odor[5]. In the current basic observational study, our first goal was to determine if this interference effect – a performance-based perceptual measure of odor imagery ability[5] – is associated with self-reported imagery ability and the decoding of odor quality from functional magnetic resonance imagining (fMRI) patterns evoked by imagined odors in the piriform cortex (Fig. 1a). Participants were instructed to imagine the smell or sight of a rose or cookie (or nothing at all) while trying to determine which

of two samples contained either the same odor (matched trial) or the other odor (mismatched trial) at their detection threshold level (Fig. 1e). Interference was calculated by subtracting detection accuracy (% trials correct) in mismatched trials from that in matched trials of each imagery condition (Fig. 1f). In line with prior work[5], an interference effect was observed for odor, but not visual, imagery (Fig. 1f). This odor interference effect correlated positively with self-reported ability to imagine odors and flavors, but not visual stimuli (Extended Data Fig. 1). Further, the difference in detection accuracy on matched versus mismatched trials of the visual imagery condition did not correlate with self-reported odor ($r_{33} = 0.306$, $p_{corrected} = 0.2205$), flavor ($r_{33} = 0.247$, $p_{corrected} = 0.4557$), or visual ($r_{33} = 0.155$, $p_{corrected} = 1.000$) imagery.

Next, we used fMRI to assess brain responses to rose and cookie odors (or clean air) interspersed with trials in which participants were instructed to imagine these same odors while sniffing clean air (Fig. 2a). Since odor quality is encoded in the primary olfactory cortex across distributed patterns of activation[10], we performed multi-voxel pattern analyses (MVPA) in left and right piriform cortex regions of interest (ROIs; Fig. 2b). Specifically, we tested whether distinct patterns for the real and/or imagined odors could be decoded using two methods: a support vector machine (Fig. 2c) and split-half voxel correlations (Fig. 2d). The decoding of actual odors in the right piriform cortex (mean accuracy = 63.2%, chance = 50%) was significantly greater than chance and significantly better than decoding in the left piriform cortex (Fig. 2e). This finding aligns with the well-documented right hemispheric dominance in olfaction[11,12]. We did not observe significant decoding of imagined odors or cross-modal decoding between the real and imagined odors (Fig. 2e–f). We note that one-third of the participants did not exhibit discriminable patterns for real odors. This is expected in decoding analyses due to natural anatomical variations[13] limiting the detection of well-known spatial olfactory codes[10,14]. Therefore, for the subsequent analyses, we tested decoding in the right piriform cortex using voxel correlations (decoding method #2) in the limited sample wherein clear discriminable patterns for real odors were observed. The results remain largely unchanged when including the full sample (Supplementary Table 1).

To determine if the decoding of imagined odor quality was associated with our perceptual measure of odor imagery ability (Fig. 1a), we correlated it against the interference effect. A strong positive association was identified (Fig. 2g). By contrast, there were no significant correlations between odor imagery and the decoding of fMRI patterns evoked during actual odor presentations or in the cross-modal datasets (Fig. 2h–i). Importantly, when we ran similar analyses for the left and right primary visual cortices as control regions, no significant

effects were observed (Extended Data Fig. 2; Supplementary Table 1). Finally, univariate responses in the piriform cortex during odor imagery (Extended Data Fig. 3) were not associated with the odor imagery measures, including after small-volume correction (no suprathreshold clusters). Collectively, these data show a strong and specific correspondence between all three measures of odor imagery ability, supporting their validity. They also demonstrate that odor imagery is associated with the successful activation of distinct imagined odor quality codes in the right piriform cortex.

We next tested whether our perceptual (i.e., the interference effect) and neural (i.e., right piriform decoding of imagined odors) measures of odor imagery ability were associated with FCR. FCR was quantified using validated measures of craving[15] and cue-potentiated intake[16], as well as ventral striatal (VS) responses to the cookie odor (Fig. 1b). First, participants rated the strength of their craving in response to the presentation of 90 palatable food images[15]. Food craving was not significantly related to the perceptual or neural measures of odor imagery ability (Fig. 3a–b) or to the decoding of actual odors in the right piriform cortex (Supplementary Table 2). However, the rated liking of the foods depicted in the pictures was variable and correlated with craving (Supplementary Table 3). We therefore reasoned that odor imagery may intensify cravings specifically for foods that are liked and constructed a linear regression model to test for the presence of an interaction between odor imagery and food liking on the average craving rating. As predicted, the interaction was significant for the perceptual measure of odor imagery ability ($F_{41} = 8.516$, $p_{corrected} = 0.0114$), but it did not survive correction for multiple comparisons for the neural measure ($F_{26} = 3.367$, $p_{corrected} = 0.1560$). Using a tertiary split to separate participants based on their average food liking, we found a strong positive association between the perceptual measure of odor imagery ability and food craving for highly liked foods (Fig. 3c). A follow-up analysis using a linear mixed effects model with the individual ratings for each of the 90 foods rather than participant averages also revealed a significant interaction effect ($F_{1,3996} = 7.571$, $p = 0.0060$) whereby cravings for liked but not disliked foods were more intense in individuals with vivid odor imagery. Collectively, these data suggest that odor imagery interacts with liking to invigorate cravings.

To assess cue-potentiated food intake, we performed a validated bogus taste test[16]. Participants were instructed to sample and compare the sensory properties of two plates of cookies. The purpose of the test (not revealed to participants) was to quantify the amount eaten. Separate linear regressions adjusted for sex (males ate more) and cookie liking ratings – which were positively correlated with the amount consumed (Supplementary Table 3) – revealed that

both the perceptual (Fig. 3d) and neural (Fig. 3e) measures of odor imagery ability were significant predictors of intake. By contrast, food craving and right piriform decoding of actual odors were unrelated to cookie consumption (Supplementary Tables 2–3), even after adjusting for sex and liking. The latter finding indicates that the association is specific to odor quality codes evoked during imagery. Finally, VS reactivity to the food odor was not related to any measure of odor imagery or perception, or to food craving or intake (all $p_{FWE\text{-}SVC}$ [family-wise error, small-volume corrected] ≥ 0.247). Thus, odor imagery was associated with behavioral measures of FCR, but not with VS reactivity.

Finally, we sought to determine if odor imagery is associated with current adiposity or change in adiposity over one year. Current adiposity was defined using BMI and body fat percentage (Fig. 1b); no significant associations were observed (Supplementary Table 4). This conflicted with the positive correlation between BMI and self-reported odor imagery ability observed in our prior study[8] (wherein body fat percentage and the perceptual and neural measures of odor imagery were not assessed). However, the variance in BMI differed significantly across the two studies (two-sample F-test for equality of variances: $F_{44,24} = 2.454$, $p = 0.0208$); with the current study including class I, II and III obesity (BMI: M = 26.12, SD = 6.81, Range = 18.32–53.44 kg/m^2 versus), and the prior study only class I (BMI: M = 24.25, SD = 4.35, Range = 17.70–34.06 kg/m^2). When we excluded the four individuals with class II/III obesity (BMI $\geq$ 35 kg/m^2) from our current sample, consistent with the prior report, a weak positive relationship emerged between BMI and the self-report measure of odor imagery ($r_{39} = 0.333$, $p_{uncorrected} = 0.0334$), suggesting that the association might be nonlinear. However, this effect did not survive correction for multiple comparisons ($p_{corrected} = 0.1002$) after further correlating BMI with the perceptual ($r_{39} = 0.222$, $p_{corrected} = 0.4872$) and neural ($r_{25} = 0.226$, $p_{corrected} = 0.7683$) measures of odor imagery. Thus, in contrast to our prediction, no significant associations were observed between current adiposity and odor imagery ability, though we cannot exclude the possibility of a nonlinear relationship with the self-report measure. Lastly, we tested for associations between olfactory perception or FCR and current adiposity. The only significant effect we observed was a negative correlation between the cookie odor detection thresholds and BMI (Supplementary Table 5). These data demonstrate that neither odor imagery ability nor FCR is related to current adiposity in our sample.

With respect to changes in adiposity (BMI or body fat percentage), no relationships were observed for any measure of odor imagery or perception (Extended Data Fig. 4; Supplementary Table 5). However, there were significant associations with FCR. Specifically, food intake

predicted change in body fat percentage (Fig. 3f), but it was not significant for change in BMI (r_{39} = 0.263, $p_{corrected}$ = 0.1928). Food craving predicted change in BMI (Fig. 3g), but not change in body fat percentage (r_{41} = 0.229, $p_{corrected}$ = 0.2804). Given the associations between odor imagery ability and FCR (Fig. 3c–e), and between FCR and changes in adiposity (Fig. 3f–g), we reasoned that there might be indirect effects[17,18] of odor imagery ability on changes in adiposity via FCR. This was in line with our *a priori* hypothesis that odor imagery strengthens FCR to in turn influence risk for weight gain (Fig. 1c–d).

Consistent with our planned analyses, both the perceptual (Fig. 4a) and neural (Fig. 4b) measures of odor imagery indirectly predicted change in body fat percentage via cue-potentiated intake. To assess the indirect effect of odor imagery on change in BMI via craving, we used moderated mediation to account for the effect of liking on the association between odor imagery ability and craving (Fig. 4c). This was an unplanned but data-driven secondary analysis, and therefore is possibly underpowered. Specifically, food liking was included as a moderator of the a-path. The index of moderated mediation – indicating whether the strength of the indirect effect between odor imagery and change in BMI via craving depended on the level of liking – was significant. This was driven by a significant conditional a × b indirect effect in individuals with high, but not low or moderate, food liking (Fig. 4c). In other words, better odor imagery ability resulted in greater changes in BMI through heightened craving in individuals who liked such high-fat/high-sugar foods. Taken together, these models provide evidence that odor imagery ability drives variation in FCR strength, which in turn influences risk for increased adiposity.

Mental imagery is thought to help optimize adaptive behavior through simulations of future actions based on past experiences[19]. Food choice depends upon a complex integration of internal and external signals[20]; imagining what to eat may contribute by enabling simulations of the predicted sensory pleasure and eventual nutritive value of eating a potential energy source. Recent preclinical work demonstrates that food odor exposure stimulates lipid metabolism, but only in fasted animals with functioning olfactory memory[21]. Perhaps olfactory memory – a key component of imagery – has the same effect on preparing the body for anticipated intake in humans and enhancing motivation for food.

Our study contributes novel insights into the neurobiology of olfaction. We demonstrated that odor imagery ability is reflected in the successful activation of imagined odor quality codes in the right piriform cortex. This finding was observed in the subset of individuals for whom the decoding of real odors could be achieved, suggesting that it was not attributable to expected

inter-subject anatomical variation limiting the ability to decode fMRI patterns in this region[13]. We also showed that risk for FCR is associated with these odor quality codes evoked during imagery but not during real perception. This specificity raises important questions about why and how quality coding differs in real and imagined olfaction, as well as why imagery rather than perceptual ability drives FCR. One possible explanation is that imagined odors only reactivate odor identity while real odors reactivate odor identity plus the coding of the physiochemical odorant properties known to occur across separate subpopulations of piriform cortex neurons[22]. Similar distinctions are observed between imagined and actual coding in other sensory modalities[23,24]. Therefore, this may account for our below-chance cross-modal decoding and lack of association between real odorant coding and the odor imagery measures.

Many conflicting associations have been reported between olfaction and current BMI or risk for weight gain in humans[25–30], including abnormal brain responses to taste and odor cues in obesity[31,32]. Here we observed a negative correlation between BMI and the cookie odor detection thresholds. Though this is a potential limitation of our study, detection thresholds do not necessarily map onto suprathreshold perceptions[33] (e.g., intensity and liking). It also is not clear how poorer detection might contribute to the indirect link between odor imagery and adiposity change via FCR that we observed. Furthermore, olfactory function or perception – defined as detection thresholds, piriform decoding of actual odor quality, and suprathreshold odor ratings – were unrelated to any measure of odor imagery ability, FCR, or adiposity change (Supplementary Tables 2–6). Thus, our results suggest that olfactory imagery and its accompanying multivariate activity patterns in the piriform cortex rather than perception *per se* may drive prospective changes in adiposity through FCR, though we cannot rule out univariate contributions from brain networks involved in related processes such as decision making, reward, and inhibition[32].

We cannot explain why neither FCR nor odor imagery ability were associated with current BMI in our study. However, it is possible that there is an unknown factor such as self-control in our sample counteracting the expected association. Likewise, a similar compensatory mechanism may account for the lack of direct effects between odor imagery ability and changes in adiposity that we observed. Future work that includes a more comprehensive assessment of resiliency factors is therefore needed. It is also important to determine if the observed effects extend to other imagined odor or flavor qualities and whether strategies aimed at intervening with odor imagery might prove to be effective targets for weight loss. Nevertheless, our findings suggest that in an environment laden with food cues, the ability to vividly imagine their smells drives overeating and craving for liked foods, which in turn promotes increased adiposity.

METHODS

Participants

The current study was classified as basic observational research in humans and did not meet the National Institutes of Health definition of a clinical trial. A flow diagram depicting the number of individuals at each stage of the study (e.g., eligibility, recruitment, completion, analysis) is provided in Extended Data Fig. 5. Participants were recruited from the local New Haven, CT, USA community and university population via flyer and social media advertisements. Individuals interested in this study or other previous studies in our lab filled out an online form using Qualtrics software versions October 2020–June 2022 (Qualtrics, Provo, UT, USA) to indicate through self-report initial information such as their sex assigned at birth, age, estimated BMI, drug use, etc. We pre-screened subjects in this database to identify individuals aged 18–45 and free from known taste or smell dysfunction, dieting behaviors, food restrictions, nicotine or drug use, serious medical conditions including metabolic, neurologic, and psychiatric disorders or medications used to treat these, cognitive deficits or memory loss that could impact mental imagery, and any MRI-contraindications (e.g., being left-handed, pregnant, or having metal in the body). We then assessed for further eligibility with follow-up email questions (e.g., to ensure that these people did not note any new disorders or drug use, recent smell loss due to COVID-19, or intent to leave the greater New Haven, CT area). To capture similar individuals across a range of BMIs, we used stratification to minimize differences in sex, race, ethnicity, age, and household income among participants recruited into 2 BMI groups (low BMI < 25 and high BMI $\geq$ 25 kg/m^2).

For the perceptual measure of odor imagery ability, 36 participants completed all imagery conditions based on an a priori power analysis performed in G*Power version 3.1.9.6[34,35] to replicate the interference effect (d = 0.722) from the prior task validation[5] in the low and high BMI groups (n = 18 each) at 0.80 power (alpha = 0.05, two-tailed test, two dependent means). Twelve additional participants were then recruited to complete only the odor imagery condition and all other study measures (with one excluded from scanning due to extreme claustrophobia). This was sufficient to achieve 0.80 power (n = 42, alpha = 0.05, two-tailed test, bivariate normal model) for the effect observed between self-reported odor imagery ability and obesity risk (r = 0.42) in previous work[8] and for the ability of FCR measures to predict longer-term changes in eating and weight (r = 0.42) from a prior meta-analysis[2]. Data from three participants were removed due to an inability to obtain proper odor thresholds such that their detection accuracies fell below chance level (less than 50% correct responses). Participant

characteristics of the final sample (N = 45) by BMI group are provided in Supplementary Table 7.

Stimuli

Odors included “phenylethyl alcohol white extra” (rose, #001059147) and “cookie dough” (cookie, #10610208) from International Flavors and Fragrances (IFF; New York, NY, USA) diluted in food-grade propylene glycol. Rose and cookie were selected for us by IFF after we requested odors that were highly volatile, discernable, and equally pleasant. We also wanted both odors to have a “sweet note,” with one being edible and one inedible. Although rose flavor is used in some food cultures, ratings of odor edibility were not significantly associated with any measure of odor imagery ability in the current study (Supplementary Table 4). Ratings of odor liking also did not significantly differ for the rose and cookie odors in our sample (Extended Data Fig. 6d). The bogus taste test consisted of eight “Grandma’s Homestyle Chocolate Chip Cookies” broken into bite-sized pieces across two plates (for a total of ~280g or ~1360 kcal) presented alongside a 16 fl oz water bottle.

Experimental Procedures

The study consisted of three behavioral sessions and one fMRI scan at baseline, along with a follow-up session one year later. Full data collection from the first (baseline) to last (follow-up) sessions spanned 10/6/2020–6/3/2022. The fMRI scan was scheduled between 8:00am-1:00pm, and all other sessions took place between 8:00am-8:00pm. We ensured that food craving and intake were assessed between the hours of 11:30am-7:00pm. Individuals were instructed to arrive to all sessions neither hungry nor full, but at least one-hour fasted. Data collection and analysis were not performed blind to the conditions of the experiments.

Behavioral Sessions

Training and Scales. Participants were first trained to make computerized ratings in PsychoPy version 3.0[36] by practicing with imagined sensations (e.g., the taste of your favorite chocolate) and real stimuli (e.g., the brightness of the ceiling light or the pressure of a weight). Intensity and liking were rated with the vertical category-ratio general Labeled Magnitude Scale (gLMS)[37–39] and Labeled Hedonic Scale (LHS)[40], respectively. The gLMS ratings were log base 10 transformed prior to any analyses. All other ratings were made on horizontal visual analog

scales (VAS). Familiarity and edibility were rated from “not at all familiar” to “more familiar than anything” and from “not at all” to “more than anything” in response to “how much do you want to eat this?”, respectively. Internal state ratings for hunger, fullness, thirst, anxiety, and need to urinate were made from “not at all [hungry/full/etc.]” to “more [hungry/full/etc.] than anything.” Subjective hunger was calculated as the difference of VAS ratings for hunger – fullness. Participants also practiced one odor run in a mock MRI simulator in the lab.

Adiposity. Body weight was measured with an electronic scale and height with a digital stadiometer to calculate BMI. Bioelectric impedance analysis (Seca Medical Body Composition Analyzer mBCA 525, Hamburg, Germany) was used to obtain body fat percentage; values were divided by 21 for females and by 31 for males to adjust for sex.

Questionnaires. Participants completed the Vividness of Olfactory Imagery[41] and Vividness of Visual Imagery[7] Questionnaires (VOIQ/VVIQ) in which they imagined odors/visual objects across 16 scenarios and rated the vividness of their mental imagery from one “perfectly clear and as vivid as normal smell/vision” to five “no image at all – you only know you are thinking of an odor/object.” Both inventories were reverse scored such that higher sums reflected larger self-reported imagery ability. Participants also did a modified Vividness of Food Imagery Questionnaire (VFIQ)[8] that was similar to the VOIQ but focused on the ability to imagine external food odors (e.g., of cookies in the oven) and flavors in the mouth (e.g., of eating cookies, which also rely on olfaction). Total weekly metabolic equivalent task-minutes (MET-minutes) from the International Physical Activity Questionnaire (IPAQ)[42] was used to assess habitual exercise. MET-minutes for each type of physical activity represent the total minutes dedicated to the activity times the estimated energy expenditure during the activity as a multiple of resting energy expenditure (e.g., vigorous activities count toward a higher MET score than moderate activities). Total score from an American version of the Dietary Fat and Free Sugar Short Questionnaire (DFS)[43] was measured to quantify high-fat/high-carbohydrate intake.

Perceptual Task of Odor Imagery Ability. Detection thresholds for the rose and cookie odors were first determined using a 16-step dilution series (4% odor by volume to 1.22ppm) in a 2-alternative forced-choice staircase procedure[44]. In a within-subjects and counterbalanced design, blindfolded participants then completed three imagery conditions (odor, visual, and none) of a validated perceptual task[5]. During odor and visual imagery, they were instructed to imagine the smell or sight of one odor type (e.g., rose) while trying to determine which of two samples “smelled stronger.” In matched trials, the two samples contained: (1) the same odor as the imagined type – e.g., rose – at their detection threshold level, and (2) the odorless propylene

glycol diluent. In mismatched trials, the two samples were: (1) the incongruent odor – e.g., cookie, and (2) the odorless diluent. In the no imagery condition, odor detection trials were performed in the absence of imagery. The odor and visual imagery conditions contained 25 matched and 25 mismatched trials per odor (100 total), and the no imagery condition consisted of 25 trials per odor (50 total), all counterbalanced for presentation order (i.e., sample one contained the odor in 50% of trials). The interference effect (perceptual measure of odor imagery ability) was calculated by subtracting detection accuracy (% trials correct) in mismatched trials from that in matched trials of the odor imagery condition. The potential presence of a visual interference effect was also determined by subtracting detection accuracy in mismatched trials from that in matched trials of the visual imagery condition. As none was observed (Fig. 1f), the "interference effect" always refers to the odor rather than visual imagery condition.

Food Cue Reactivity. Cue-induced craving strength was rated in response to 90 palatable food pictures[15] on a horizontal VAS from "I do not want it at all" to "I crave it more than anything," and the average was calculated. Items included familiar American snacks and meals, such as pizza and doughnuts. For cue-potentiated intake, participants completed a bogus taste test[16] in which they were instructed to eat as much as they liked while comparing the sensory properties of two plates of cookies (e.g., which tastes sweeter/saltier, is fresher, or has better quality chocolate). They were not explicitly told that the cookies were identical and that the primary aim was to quantify the grams consumed. Data from two participants were excluded from this measure after eating more than 3 SD above the group mean. Following the food craving and intake paradigms, participants also rated their liking on the LHS[40] and frequency of consumption in a typical month on a VAS (labels: 1 or less/month, 2/month, 3/month, 1/week, 2/week, 3–4/week, 5–6/week, 1/day, 2 or more/day) for each stimulus.

fMRI Session

Participants underwent fMRI scanning while performing a task in an event-related design with six trial types: smell rose, cookie, or clean air; and imagine rose, cookie, or clean air. Each trial began with a 5s auditory cue of "smell" or "imagine" followed by the name of the odor (e.g., "rose") and the countdown "three, two, one, sniff." We instructed participants to sniff in each trial prompted by the auditory cue to equate attentional demands. Odor/clean air delivery (3s) was time-locked to sniff onset. Trials were separated by intertrial intervals of 7–17s (mean = 10s). Participants completed 30 pseudorandomized trials per run (five of each type) and five runs per scan. Runs were ~9min long and separated by ~2min breaks to minimize olfactory habituation.

Stimuli were delivered at concentrations matching individual ratings of moderate intensity on the gLMS with a custom MRI-compatible olfactometer that has been described in detail previously[45] (also see the Supplementary Methods).

fMRI data were acquired with a Siemens 3 Tesla Magnetom Prisma scanner using a 32-channel head coil. Images were collected at an angle of 30° off AC-PC to reduce susceptibility artifacts in olfactory regions. Sagittal T1 anatomical images (repetition time TR = 1900ms, echo time TE = 2.52ms, 176 slices, field of view FOV = 250mm, voxel size = 1×1×1mm) and functional echo-planar images (EPIs) with a multiband blood-oxygen-level dependent (BOLD) sequence (TR = 2100ms, TE = 40ms, 72 slices, flip angle = 85°, FOV = 192mm, voxel size = 1.5×1.5×1.5mm, multiband acceleration factor = 4) were obtained.

Follow-Up Session

The primary goal of the follow-up session was to assess changes in adiposity. All but one participant returned to the lab approximately one year later (days elapsed from first to last session: M = 363.17, SD = 7.33, range = 340 – 378) and repeated the adiposity, questionnaire, and FCR measures, but not the odor imagery measures. Follow-up data from one participant was excluded after they began a strict diet and lost more than 3 SD above the group mean in weight change from the baseline to follow-up sessions.

Data Analyses

Behavioral Analyses

Pearson correlations, linear regressions, linear mixed effects models, ANOVAs, and Student's t-tests were performed in MATLAB 2020a (Mathworks, Natick, Massachusetts, USA). For ANOVAs assessing the interaction of two variables, we included in the model each of the two variables independently, the interaction of the two, and any control variables indicated in the text. Variables of interest with outliers > 3 SD above or below the group mean were removed if they changed the nature of the results. Data distribution was assumed to be normal, but this was not formally tested. All statistical tests were two-sided. Corrections for multiple comparisons were made by adjusting the p-value for the number of tests at each step using the Bonferroni method. The only exception was in determining variables that should be included as covariates. In these limited cases (e.g., the associations between food intake and sex or food liking), correction for multiple comparisons was not performed to err on the side of caution. Data were plotted in Prism version 9.4.1 (GraphPad Software, San Diego, CA, USA). For test-retest

reliability, intraclass correlation coefficient estimates and 95% CIs were calculated in SPSS based on single measure, absolute agreement, 2-way mixed models. All measures showed moderate to good reliability (Supplementary Table 8). For details of the sniff analyses (reported in Extended Data Fig. 7 and Supplementary Table 9), see the Supplementary Methods.

Mediation and moderated mediation models were tested with bootstrapping (10000 samples, 95% CIs) using the "PROCESS" macro version 4.1[46] models 4 and 7 implemented in SPSS Statistics version 28 (IBM, Chicago, IL, USA). Significant effects were supported by confidence intervals (CIs) excluding zero within the lower and upper bounds. The selection of these models is described in the Supplementary Methods.

fMRI Analyses

Preprocessing. The fMRI data were preprocessed and analyzed using FSL version 5.0.10 (FMRIB Software Library, Oxford, UK[47] and SPM12 (Statistical Parametric Mapping, Wellcome Centre for Human Neuroimaging, London, UK) implemented in MATLAB R2019b. Functional EPIs were realigned to the mean and unwarped using fieldmaps, slice-time corrected, and motion-corrected with the FSL tool MCFLIRT[48]. The anatomical T1 image was coregistered to the mean EPI and spatially normalized to the standard MNI-152 reference with unified segmentation in SPM12. Prior to the univariate analyses, the resulting nonlinear deformation fields were applied to the EPI images, which were then smoothed with a 3mm full-width-half-maximum Gaussian kernel.

First Level Models. General linear models (GLMs) were estimated for each participant and run, separately for the normalized and smoothed EPI data (for univariate analyses) and the non-normalized and non-smoothed EPI data (for decoding analyses). In each, the 6 trial types (smell rose/cookie/clean air and imagine rose/cookie/clean air) were modeled with a canonical hemodynamic response function as events of interest with onsets time-locked to the start of odor/clean air delivery and durations of 3s. The following nuisance regressors were also included: 24 motion parameters (the six SPM realignment parameters for the current volume, six for the preceding volume, plus each of these values squared[49], the mean signal extracted from the ventricular cerebrospinal fluid computed with *fslmeants*, a matrix of motion-outlier volumes identified using *fsl_motion_outliers* (threshold = 75th percentile plus 2.5 times the interquartile range and/or greater than 1mm of framewise displacement[50]), and the preprocessed sniff trace down-sampled to the scanner temporal resolution with decimation. A 128s high-pass filter was applied to remove low-frequency noise and slow signal drifts.

Univariate Analyses. As there was no main effect of odor type (rose/cookie) on fMRI activity (p_{FWE} [cluster-level family-wise error corrected across the whole brain] ≥ 0.3214), we collapsed across the odorants in the subsequent univariate analyses (Extended Data Fig. 3 and Supplementary Tables 10–13), aside from testing VS reactivity to smelling the food odor. The following contrast images were created at the single-subject level and averaged across the five runs: smell odor (rose + cookie) > smell clean air, imagine odor > imagine clean air, imagine odor > smell clean air, smell odor > imagine odor, and imagine odor > smell odor. The contrasts of smell cookie > smell rose and smell cookie > smell clean air were also created toward assessing VS reactivity.

Group-level random effects analyses were conducted with one-sample t-tests thresholded at $p_{uncorrected} < 0.001$ and a cluster size of at least five contiguous voxels. Conjunction analyses were performed for the contrasts smell odor > smell clean air and imagine odor > imagine clean air using the conjunction null hypothesis. Effects were considered significant at $p_{FWE} < 0.05$. We also regressed the perceptual measure of odor imagery ability (i.e., the interference effect) against whole-brain BOLD responses to imagining odors > imagining clean air, imagining odors > smelling clean air, and imagining odors > smelling odors. Here we considered whole-brain effects and those significant in the piriform cortex at a peak-level of $p_{FWE\text{-}SVC} < 0.05$, family-wise error small-volume corrected for multiple comparisons in our two ROIs (see below). The $p_{FWE\text{-}SVC}$ values were subsequently Bonferroni corrected for the two SVC searches. Finally, for VS reactivity, we regressed variables of interest against whole-brain BOLD responses in the contrasts of smelling cookie > smelling rose and smelling cookie > smelling clean air. We considered effects significant in a bilateral ventral striatum mask derived from Bartra et al. ("positive > negative effects of subjective valuation on BOLD")[51] at $p_{FWE\text{-}SVC} < 0.05$. The anatomical labels were determined jointly from the "Atlas of the Human Brain"[52], an adult maximum probability atlas prepared with SPM12 (www.brain-development.org)[53], and the Automated Anatomical Labeling Atlas 3[54].

Decoding Analyses. The ROIs for the decoding analyses included the left and right piriform cortices independently created from the Neurosynth[55] meta-analytic functional map for the term "olfactory" (74 studies with 2021 activations, downloaded 9/15/2021). Activations from this map were restricted to a threshold of z = 6 to ensure separability of the piriform clusters from other nearby regions (e.g., the insula). Control regions for the decoding analyses included the left and right primary visual cortices from the Automated Anatomical Labeling Atlas 3[54] ("calcarine fissure and surrounding cortex"). The ROIs and control regions were converted from

MNI space to each subject's native EPI space (voxel size = 1.5×1.5×1.5mm). This resulted in clusters of 190 and 111 voxels for the left and right piriform ROIs, respectively.

MVPA was performed using The Decoding Toolbox[56] version 3.999E implemented in SPM12. For the first decoding method (support vector machine or SVM classification), separate voxel-wise patterns were created for smelling and imagining the rose and cookie odors by extracting the parameter estimates from the first level GLMs and subtracting the mean activity across the conditions in each run. This resulted in one rose and one cookie fMRI pattern per condition and run (e.g., smell rose and smell cookie) for training or testing in a cross-validated approach. Feature selection was used to identify the top class-discriminative voxels in each ROI or control region with an ANOVA, restricted to the number of voxels in each ROI maximally available for all subjects. An SVM from the Library for Support Vector Machines (LIBSVM) package[57] was trained to decode rose versus cookie using patterns of BOLD activation for smelling the odors in four of five scan runs. The SVM was then tested for its accuracy to predict these odor types from the patterns in the left-out run. These steps were repeated for training and testing on the imagined odor patterns, and for training on smelled odors and testing on imagined odors (and vice versa, averaged for the cross-modal condition). SVM accuracies were compared to chance (50%) in one-sample t-tests to assess group-level significance. SVM accuracies for the decoding of real odors in the left versus right piriform cortex were also directly compared with a paired-samples t-test to assess the laterality of the effect.

While reliable and a standard approach, this form of run-wise MVPA provides a relatively insensitive outcome metric that is not well-suited for correlation analyses (see the Supplementary Methods). For a more sensitive measure, we used a second decoding method: split-half voxel correlations. The first BOLD run was treated as an odor localizer, which resulted in an equivalent number of even and odd runs remaining for decoding (2 each). The voxels for each subject and ROI or control region were functionally ranked according to their t values in the contrast of smelling odor > smelling clean air from the localizer. Again, the N-most odor-active voxels maximally available for all subjects were selected. The split-half voxel correlations were then analyzed for the within-odor (e.g., smelling rose in even runs versus smelling rose in odd runs) minus the between-odor (e.g., smelling rose in even runs versus smelling cookie in odd runs) fMRI patterns in each ROI or control region. In line with our SVM analyses, we performed separate tests for real, imagined, and cross-modal odors. The resulting correlation values were Fisher's Z transformed and compared to zero in one-sample t-tests to assess group-level significance. They were also tested in correlations against the perceptual measure

of odor imagery ability. The latter analyses were performed in all individuals and separately restricted to those with discriminable neural patterns for actual odors in each ROI or control region, defined as within-odor minus between-odor voxel correlation Z-values > 0. See the Supplementary Methods for our reasoning behind this restriction.

Inclusion and Ethics Statement

Where applicable, this research conforms to the recommendations of the Global Code of Conduct. All participants provided written informed consent and were compensated. The study was conducted in accordance with the standards laid out in the Declaration of Helsinki. The study procedures were approved by the Yale Human Investigations Committee (Institutional Review Board Protocol #0405026766). The study was also preregistered on January 20, 2021, to AsPredicted.org under access #56278, available at: https://aspredicted.org/by3yb.pdf.

DATA AVAILABILITY

The raw MRI data and sniff airflow traces can be downloaded from the OpenNEURO repository under accession #ds004327 at: doi:10.18112/openneuro.ds004327.v1.0.1. Statistical maps of the human brain data are available on the NeuroVault repository at: https://neurovault.org/collections/14751/. All other data analyzed in this study are included in the source data files provided with this paper.

CODE AVAILABILITY

Custom code used in data collection and analysis is available at: https://github.com/eeperszyk/odor-imagery.

ACKNOWLEDGEMENTS

This work was supported by the National Science Foundation Graduate Research Fellowship under Grant No. 2139841 (E.E.P.), the National Institute of Diabetes and Digestive and Kidney Diseases of the National Institutes of Health under Award No. F31DK130556 (E.E.P.), and the Modern Diet and Physiology Research Center (D.M.S.). The content is solely the responsibility of the authors and does not necessarily represent the official views of the National Science Foundation or the National Institutes of Health. We would like to thank Jason Avery for advice on the fMRI decoding methods; Bojana Kuzmanovic for guidance on the fMRI preprocessing pipeline; James Howard for example code to perform the sniffing analyses; Thomas Hummel,

Johan Lundström, Joel Mainland, and Paul Wise for their thoughts in troubleshooting the odor detection threshold testing; Alain Dagher, Ralph DiLeone, and Barry Green for their helpful suggestions to the project design and analyses; and Karen Martin for MR technical assistance.

AUTHOR CONTRIBUTIONS STATEMENT

Conceptualization, E.E.P. and D.M.S.; Methodology, E.E.P., X.S.D., J.D., M.J-G., J.T., Z.H., M.G.V., L.K., T.D.W., H.K., and D.M.S.; Formal Analysis, E.E.P., L.K., and X.S.D.; Investigation, E.E.P. and J.T.; Resources, X.S.D., J.D., M.J-G., Z.H., M.G.V., L.K., T.D.W., H.K., and D.M.S.; Data Curation, E.E.P.; Writing – Original Draft, E.E.P. and D.M.S.; Writing – Review & Editing, X.S.D., J.D., M.J-G., J.T., Z.H., M.G.V., L.K. T.D.W., and H.K.; Visualization, E.E.P.; Supervision, X.S.D., H.K., and D.M.S.; Funding Acquisition, E.E.P. and D.M.S.

COMPETING INTERESTS STATEMENT

The authors declare no competing interests.

FIGURE LEGENDS

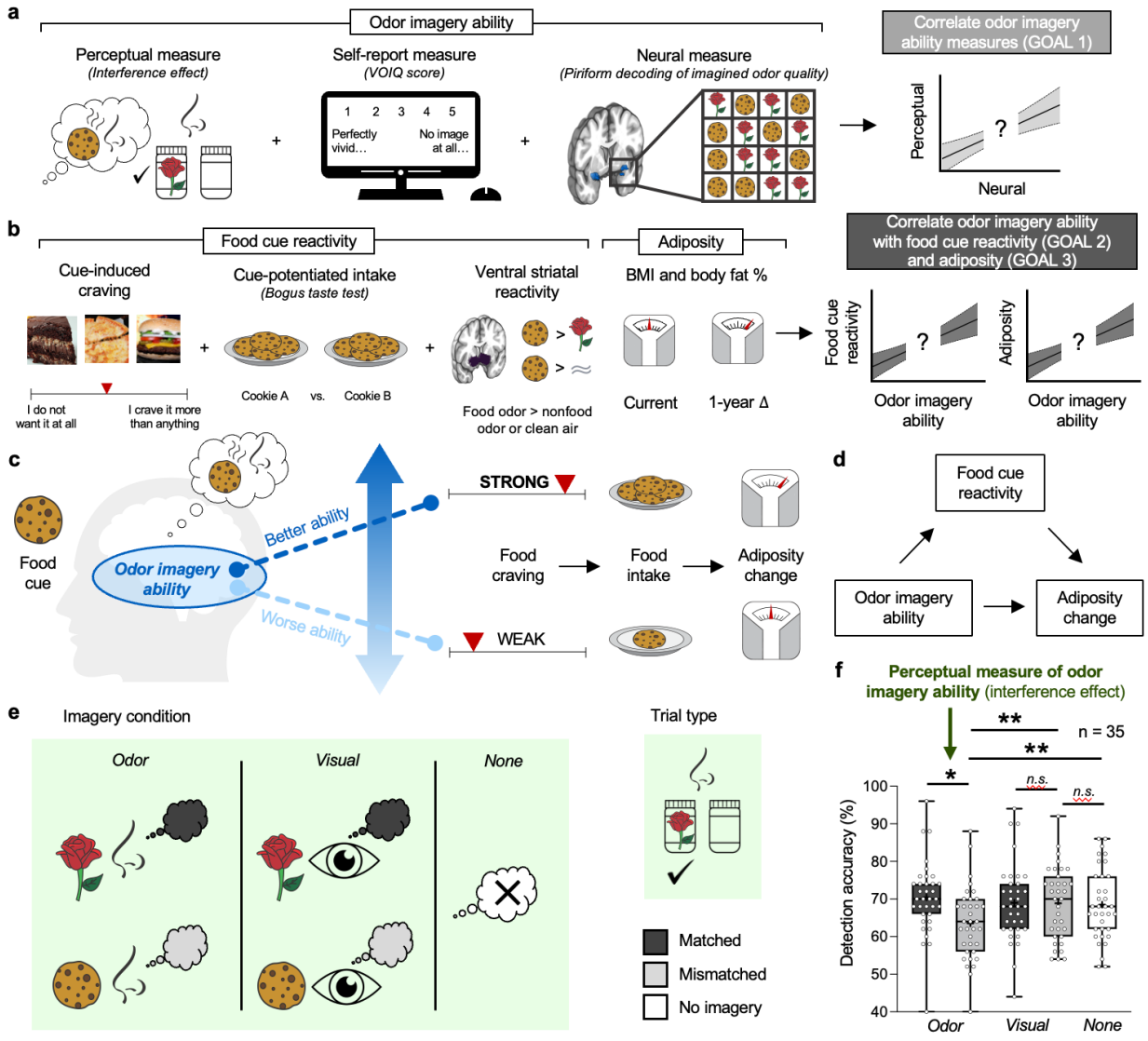

Fig. 1: Study overview and the perceptual measure of odor imagery ability.

(a) Our first goal was to correlate three measures of odor imagery ability: a validated perceptual measure[5], a self-report measure (the Vividness of Olfactory Imagery Questionnaire or VOIQ[41]), and a new neural measure based upon the piriform decoding of imagined odor quality.

(b) Our second goal was to correlate odor imagery ability with three measures of FCR: cue-induced craving from an established paradigm[15], cue-potentiated intake in a bogus taste test[16], and ventral striatal reactivity to a food odor versus a nonfood odor or clean air. Our third goal was to correlate odor imagery ability with both current and one-year changes in adiposity.

(c) We hypothesized that in response to learned food cues, individuals with a better ability to imagine odors would experience stronger cravings that compel them to overeat and gain weight. In contrast, individuals with a worse ability to imagine odors would experience weaker cravings that have a low impact on their eating and weight.

(d) We predicted that odor imagery ability would have an indirect effect on adiposity change via FCR.

(e) In the adapted perceptual task[5] to quantify odor imagery ability, participants were instructed to imagine the smell or sight of a rose/cookie or nothing at all while trying to detect either the same (matched trial) or the other (mismatched trial) odor at their detection threshold level (determined prior to the test).

(f) As in previous work[5], we found that odor imagery impairs mismatched odor detection without improving matched detection (i.e., the "interference effect") using two-sided tests (t-statistics) of fixed effects in linear mixed effects models. See the Supplementary Results for further analyses behind establishing this perceptual measure of odor imagery ability. Box-and-whisker plots represent single participants from the minimum to maximum (whiskers) around the 25^{th} to 75^{th} percentiles (box limits), along with the median (center line) and mean (+ symbol) of the data. *n.s.*, not significant. *post-hoc pairwise comparisons: $p_{corrected} < 0.05$ (2 tests comparing odor or visual matched versus mismatched detection); **post-hoc pairwise comparisons: $p_{corrected} < 0.05$ (3 tests comparing odor mismatched, visual mismatched, and no imagery detection).

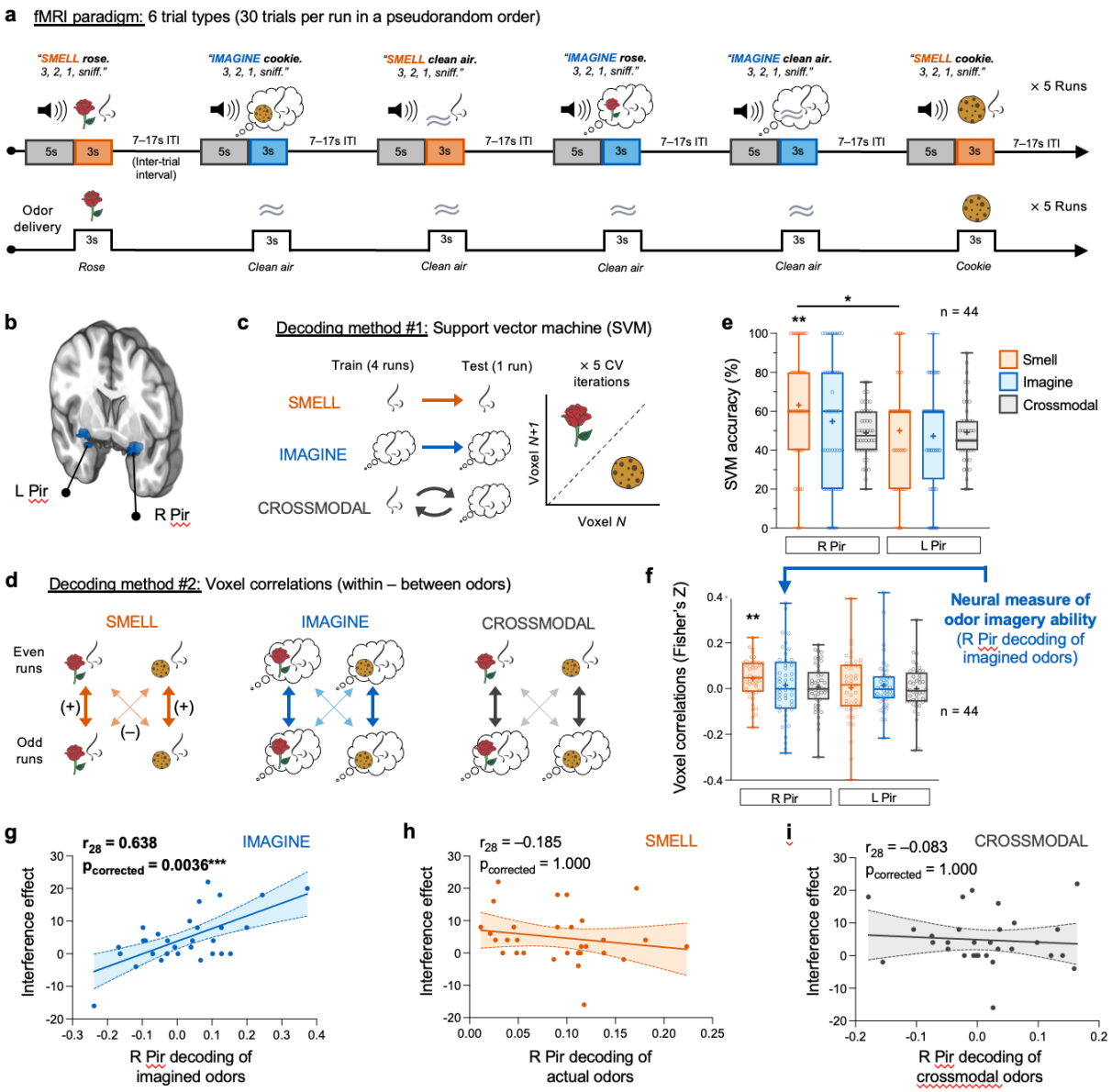

Fig. 2: Decoding of imagined, but not actual, odors in the right piriform cortex provides a neural measure of odor imagery ability.

(a) Overview of the fMRI paradigm. After an auditory cue, participants either smelled rose or cookie odors (or clean air) or imagined these odors while sniffing clean air.

(b) Decoding ROIs.

(c) For the first decoding method, support vector machines (SVMs) were trained and tested to classify rose versus cookie over five cross-validated (CV) iterations. In the "smell/imagine odor" conditions, SVMs were trained and tested on voxel patterns from the same modality. For cross-modal decoding, the SVM was trained and tested on real versus imagined patterns.

(d) For the second decoding method, split-half Fisher's Z-transformed voxel correlations calculated between-odors (e.g., smelling rose in even runs versus smelling cookie in odd runs) were subtracted from those calculated within-odors (e.g., smelling rose in even versus odd runs).

(e–f) SVM accuracies (e) and voxel correlations (f) for smelling actual odors were only significant in the right piriform cortex at the group-level (t_{43} = 2.991, $p_{corrected}$ = 0.0184; t_{43} = 3.342, $p_{corrected}$ = 0.0056). SVM accuracies were also significantly greater in the right than left piriform cortices (t_{43} = 2.407, p = 0.0205). Neither decoding measure was significant for imagined or cross-modal odors in the ROIs tested.

(g–i) The perceptual measure of odor imagery correlated with right piriform decoding of imagined (g), but not real (h) or cross-modal (i), odors using voxel correlations. Right piriform decoding of imagined odors was unrelated to any demographics, olfactory function or perception, sniff parameters, hunger, or dietary habits (Supplementary Table 4).

Box-and-whisker plots represent single participants from the minimum to maximum (whiskers) around the 25th to 75th percentiles (box limits), along with the median (center line) and mean (+ symbol) of the data. Scatterplots depict single participants and the 95% CI around the line of best fit. Linear relationships were tested with two-tailed Pearson's r correlations. L, left; R, right; Pir, piriform cortex. *p < 0.05 test for laterality; **$p_{corrected}$ < 0.05 (4 tests per condition across the 2 ROIs + 2 control regions; see Extended Data Fig. 2); ***$p_{corrected}$ < 0.05 (18 tests comparing decoding versus the interference effect; see Supplementary Table 1).

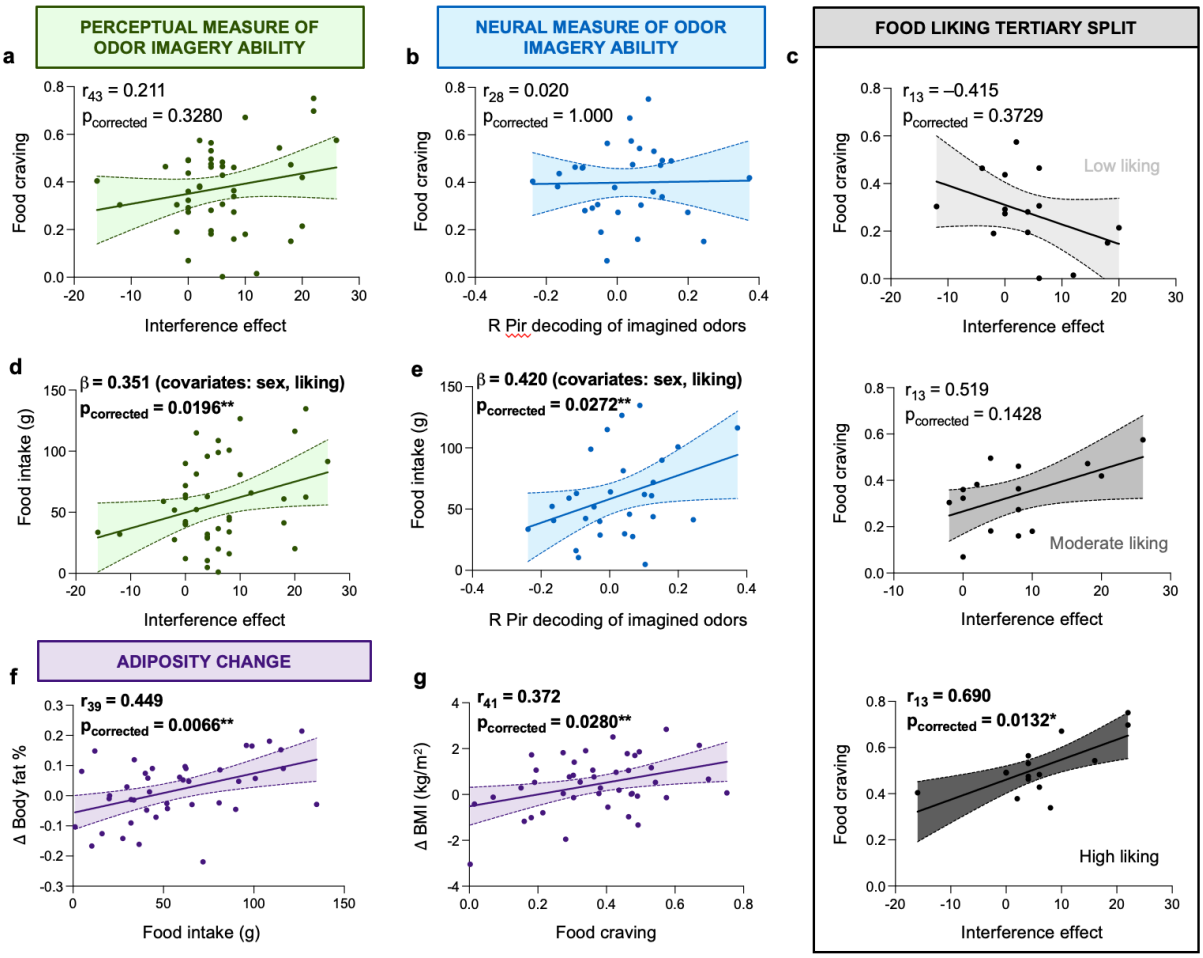

Fig. 3: Better odor imagery ability is associated with stronger cravings for liked foods and greater intake.

(a–b) Food craving did not correlate with the perceptual (a) or neural (b) measures of odor imagery ability.

(c) There was a significant interaction between food liking and the perceptual measure of odor imagery ability on craving ($p_{corrected}$ = 0.0114). Following a tertiary split to separate participants by their average food liking, the interference effect was unrelated to food craving in the low and moderate food liking groups. By contrast, there was a positive correlation in the high food liking group. In addition, accounting for subjective hunger ratings – which were positively correlated with food craving (Supplementary Table 3) – did not impact the results. No other variables of interest were associated with food craving (Supplementary Tables 2–3). Low liking group: mean LHS rating = –0.17, range = –66.60 to 11.68; Moderate liking group: mean LHS rating = 19.52, range = 11.83 to 27.98; High liking group: mean LHS rating = 37.69, range = 29.85 to 48.98.

(d–e) Both the perceptual (d) and neural (e) measures of odor imagery were significant predictors of cue-potentiated food intake adjusted for sex (males ate more) and cookie liking ratings, which were positively correlated with the amount consumed (Supplementary Table 2). No other variables of interest were associated with intake (Supplementary Tables 2–3).

(f–g) Food intake positively correlated with change in body fat percentage (f), whereas food craving positively correlated with change in BMI (g). Accounting for age – which was positively associated with change in BMI (Supplementary Table 6) – did not impact these results. Changes in adiposity were also unrelated to sex, household income, olfactory function or perception, food liking, dietary habits, or changes in physical activity over the year (Supplementary Tables 5–6).

Scatterplots depict single participants and the 95% CI around the line of best fit. Linear relationships were tested with two-tailed Pearson's r correlations. R, right; Pir, piriform; LHS, Labeled Hedonic Scale[40]. *post-hoc comparison: $p_{corrected} < 0.05$ (3 tests comparing food craving to the interference effect after the tertiary split for food liking); **$p_{corrected} < 0.05$ (2 tests per measure of FCR or adiposity change).

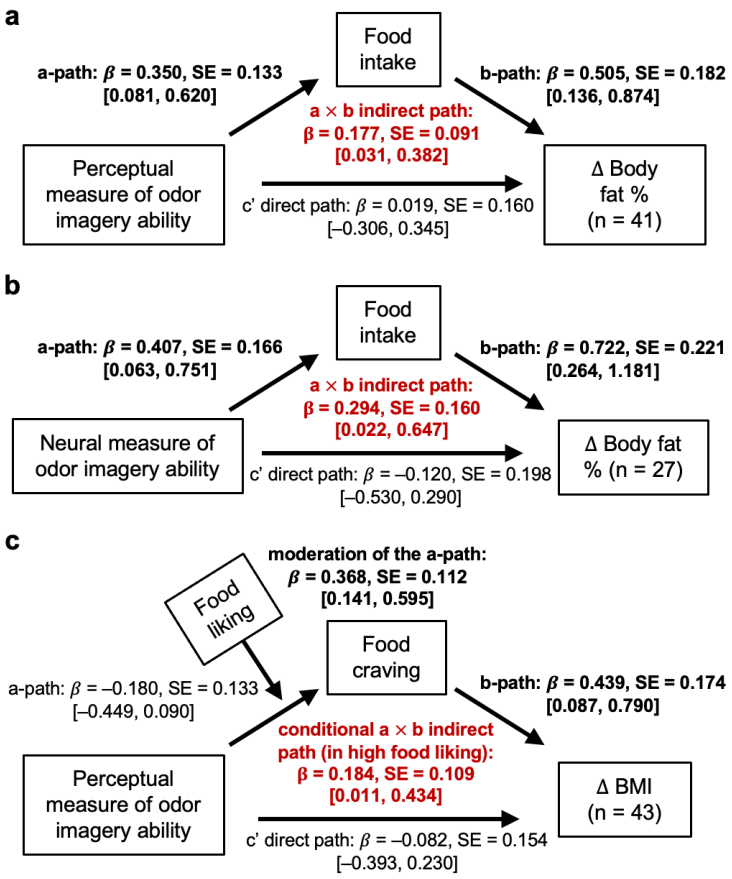

Fig. 4: Odor imagery ability indirectly predicts changes in BMI and body fat percentage via food cue reactivity.

(a–b) Testing the mediation models for the perceptual (a) and neural (b) measures of odor imagery ability revealed no direct effects between odor imagery ability and change in body fat percentage. By contrast, the indirect effects via intake were significant. These models were controlled for sex and cookie liking since these were the only variables of interest correlated with food intake (Supplementary Tables 2–3).

(c) Testing the moderated mediation model for the perceptual measure of odor imagery ability again revealed no direct effect of odor imagery ability on change in BMI. However, the index of moderated mediation was significant (β = 0.161, SE = 0.104, CI [0.007, 0.441]). This was driven by a significant conditional a × b indirect effect in individuals with high, but not with low (β = –0.079, SE = 0.103, CI [–0.347, 0.055]) or moderate (β = 0.033, SE = 0.103, CI [–0.347, 0.158]), food liking. This model was controlled for hunger (with food liking included as a moderator of the a-path) since these were the only variables of interest correlated with food craving (Supplementary Tables 2–3).

Bold font denotes significant effects at $p < 0.05$ according to CIs [lower limit, upper limit] excluding zero. Significant indirect effects are further highlighted in red.

REFERENCES

1. Hendrikse, J. J. *et al.* Attentional biases for food cues in overweight and individuals with obesity: a systematic review of the literature. *Obesity Reviews* **16**, 424–432 (2015).
2. Boswell, R. G. & Kober, H. Food cue reactivity and craving predict eating and weight gain: a meta-analytic review. *Obes Rev* **17**, 159–177 (2016).
3. Kavanagh, D. J., Andrade, J. & May, J. Imaginary Relish and Exquisite Torture: The Elaborated Intrusion Theory of Desire. *Psychological Review* **112**, 446–467 (2005).
4. Schifferstein, H. N. J. Comparing Mental Imagery across the Sensory Modalities. *Imagination, Cognition and Personality* **28**, 371–388 (2009).
5. Djordjevic, J., Zatorre, R. J., Petrides, M. & Jones-Gotman, M. The Mind's Nose: Effects of Odor and Visual Imagery on Odor Detection. *Psychol Sci* **15**, 143–148 (2004).
6. Bensafi, M. & Rouby, C. Individual Differences in Odor Imaging Ability Reflect Differences in Olfactory and Emotional Perception. *Chem Senses* **32**, 237–244 (2007).
7. Marks, D. F. Visual Imagery Differences in the Recall of Pictures. *British Journal of Psychology* **64**, 17–24 (1973).
8. Patel, B. P., Aschenbrenner, K., Shamah, D. & Small, D. M. Greater perceived ability to form vivid mental images in individuals with high compared to low BMI. *Appetite* **91**, 185–189 (2015).
9. Djordjevic, J., Zatorre, R. J., Petrides, M., Boyle, J. A. & Jones-Gotman, M. Functional neuroimaging of odor imagery. *NeuroImage* **24**, 791–801 (2005).
10. Howard, J. D., Plailly, J., Grueschow, M., Haynes, J.-D. & Gottfried, J. A. Odor quality coding and categorization in human posterior piriform cortex. *Nature Neuroscience* **12**, 932–938 (2009).
11. Zatorre, R. J., Jones-Gotman, M., Evans, A. C. & Meyer, E. Functional localization and lateralization of human olfactory cortex. *Nature* **360**, 339–340 (1992).
12. Zatorre, R. J. & Jones-Gotman, M. Human olfactory discrimination after unilateral frontal or temporal lobectomy. *Brain* **114A**, 71–84 (1991).
13. Wei, C.-S. *et al.* Editorial: Inter- and Intra-subject Variability in Brain Imaging and Decoding. *Frontiers in Computational Neuroscience* **15**, (2021).
14. Stettler, D. D. & Axel, R. Representations of Odor in the Piriform Cortex. *Neuron* **63**, 854–864 (2009).
15. Boswell, R. G., Sun, W., Suzuki, S. & Kober, H. Training in cognitive strategies reduces eating and improves food choice. *PNAS* **115**, E11238–E11247 (2018).

16. Robinson, E. *et al.* The bogus taste test: Validity as a measure of laboratory food intake. *Appetite* **116**, 223–231 (2017).
17. O'Rourke, H. P. & MacKinnon, D. P. Reasons for Testing Mediation in the Absence of an Intervention Effect: A Research Imperative in Prevention and Intervention Research. *J Stud Alcohol Drugs* **79**, 171–181 (2018).
18. Preacher, K. J. & Hayes, A. F. SPSS and SAS procedures for estimating indirect effects in simple mediation models. *Behavior Research Methods, Instruments, & Computers* **36**, 717–731 (2004).
19. Moulton, S. T. & Kosslyn, S. M. Imagining predictions: mental imagery as mental emulation. *Philosophical Transactions of the Royal Society B: Biological Sciences* **364**, 1273–1280 (2009).
20. de Araujo, I. E., Schatzker, M. & Small, D. M. Rethinking Food Reward. *Annual Review of Psychology* **71**, 139–164 (2020).
21. Tsuneki, H. *et al.* Food odor perception promotes systemic lipid utilization. *Nat Metab* **4**, 1514–1531 (2022).
22. Gottfried, J. A., Winston, J. S. & Dolan, R. J. Dissociable Codes of Odor Quality and Odorant Structure in Human Piriform Cortex. *Neuron* **49**, 467–479 (2006).
23. Ganis, G., Thompson, W. L. & Kosslyn, S. M. Brain areas underlying visual mental imagery and visual perception: an fMRI study. *Cognitive Brain Research* **20**, 226–241 (2004).
24. Steel, A., Billings, M. M., Silson, E. H. & Robertson, C. E. A network linking scene perception and spatial memory systems in posterior cerebral cortex. *Nat Commun* **12**, 2632 (2021).
25. Perszyk, E. E., Davis, X. S. & Small, D. M. Olfactory decoding is positively associated with ad libitum food intake in sated humans. *Appetite* **180**, 106351 (2023).
26. Stafford, L. D. & Whittle, A. Obese Individuals Have Higher Preference and Sensitivity to Odor of Chocolate. *Chem Senses* **40**, 279–284 (2015).
27. Han, P., Chen, H. & Hummel, T. Brain Responses to Food Odors Associated With BMI Change at 2-Year Follow-Up. *Frontiers in Human Neuroscience* **14**, 402 (2020).
28. Patel, Z. M., DelGaudio, J. M. & Wise, S. K. Higher Body Mass Index Is Associated with Subjective Olfactory Dysfunction. *Behavioural Neurology* **2015**, e675635 (2015).
29. Sun, X. *et al.* Basolateral Amygdala Response to Food Cues in the Absence of Hunger Is Associated with Weight Gain Susceptibility. *J. Neurosci.* **35**, 7964–7976 (2015).

30. Poessel, M. *et al.* Brain response to food odors is not associated with body mass index and obesity-related metabolic health measures. *Appetite* 105774 (2021) doi:10.1016/j.appet.2021.105774.
31. Han, P., Roitzsch, C., Horstmann, A., Pössel, M. & Hummel, T. Increased Brain Reward Responsivity to Food-Related Odors in Obesity. *Obesity* **29**, 1138–1145 (2021).
32. Li, G. *et al.* Brain functional and structural magnetic resonance imaging of obesity and weight loss interventions. *Mol Psychiatry* **28**, 1466–1479 (2023).
33. Dalton, P. Odor Perception and Beliefs about Risk. *Chemical Senses* **21**, 447–458 (1996).
34. Faul, F., Erdfelder, E., Lang, A.-G. & Buchner, A. G*Power 3: A flexible statistical power analysis program for the social, behavioral, and biomedical sciences. *Behavior Research Methods* **39**, 175–191 (2007).
35. Faul, F., Erdfelder, E., Buchner, A. & Lang, A.-G. Statistical power analyses using G*Power 3.1: Tests for correlation and regression analyses. *Behavior Research Methods* **41**, 1149–1160 (2009).
36. Peirce, J. W. PsychoPy—Psychophysics software in Python. *Journal of Neuroscience Methods* **162**, 8–13 (2007).
37. Bartoshuk, L. M. *et al.* Valid across-group comparisons with labeled scales: the gLMS versus magnitude matching. *Physiology & Behavior* **82**, 109–114 (2004).
38. Green, B. G., Shaffer, G. S. & Gilmore, M. M. Derivation and evaluation of a semantic scale of oral sensation magnitude with apparent ratio properties. *Chemical Senses* **18**, 683–702 (1993).
39. Green, B. G. *et al.* Evaluating the 'Labeled Magnitude Scale' for Measuring Sensations of Taste and Smell. *Chemical Senses* **21**, 323–334 (1996).
40. Lim, J., Wood, A. & Green, B. G. Derivation and Evaluation of a Labeled Hedonic Scale. *Chem Senses* **34**, 739–751 (2009).
41. Gilbert, A., Voss, M. & Kroll, J. Vividness of olfactory mental imagery: correlations with sensory response and consumer behavior. *Chem Senses* **22**, 686 (1997).
42. Hagströmer, M., Oja, P. & Sjöström, M. The International Physical Activity Questionnaire (IPAQ): a study of concurrent and construct validity. *Public Health Nutrition* **9**, 755–762 (2006).
43. Francis, H. & Stevenson, R. Validity and test–retest reliability of a short dietary questionnaire to assess intake of saturated fat and free sugars: a preliminary study. *Journal of Human Nutrition and Dietetics* **26**, 234–242 (2013).

44. Doty, R. L. Office Procedures for Quantitative Assessment of Olfactory Function. *American Journal of Rhinology* **21**, 460–473 (2007).
45. Small, D. M., Veldhuizen, M. G., Felsted, J., Mak, Y. E. & McGlone, F. Separable Substrates for Anticipatory and Consummatory Food Chemosensation. *Neuron* **57**, 786–797 (2008).
46. Hayes, A. F. *Introduction to Mediation, Moderation, and Conditional Process Analysis, Second Edition: A Regression-Based Approach*. (Guilford Publications, 2017).
47. Jenkinson, M., Beckmann, C. F., Behrens, T. E. J., Woolrich, M. W. & Smith, S. M. FSL. *NeuroImage* **62**, 782–790 (2012).
48. Jenkinson, M., Bannister, P., Brady, M. & Smith, S. Improved Optimization for the Robust and Accurate Linear Registration and Motion Correction of Brain Images. *NeuroImage* **17**, 825–841 (2002).
49. Friston, K. J., Williams, S., Howard, R., Frackowiak, R. S. J. & Turner, R. Movement-Related effects in fMRI time-series. *Magnetic Resonance in Medicine* **35**, 346–355 (1996).
50. Power, J. D., Barnes, K. A., Snyder, A. Z., Schlaggar, B. L. & Petersen, S. E. Spurious but systematic correlations in functional connectivity MRI networks arise from subject motion. *NeuroImage* **59**, 2142–2154 (2012).
51. Bartra, O., McGuire, J. T. & Kable, J. W. The valuation system: A coordinate-based meta-analysis of BOLD fMRI experiments examining neural correlates of subjective value. *NeuroImage* **76**, 412–427 (2013).
52. Mai, J. K., Majtanik, M. & Paxinos, G. *Atlas of the Human Brain*. (Academic Press, 2015).
53. Hammers, A. *et al.* Three-dimensional maximum probability atlas of the human brain, with particular reference to the temporal lobe. *Human Brain Mapping* **19**, 224–247 (2003).
54. Rolls, E. T., Huang, C.-C., Lin, C.-P., Feng, J. & Joliot, M. Automated anatomical labelling atlas 3. *NeuroImage* **206**, 116189 (2020).
55. Yarkoni, T., Poldrack, R. A., Nichols, T. E., Van Essen, D. C. & Wager, T. D. Large-scale automated synthesis of human functional neuroimaging data. *Nat Methods* **8**, 665–670 (2011).
56. Hebart, M. N., Görgen, K. & Haynes, J.-D. The Decoding Toolbox (TDT): a versatile software package for multivariate analyses of functional imaging data. *Front. Neuroinform.* **8**, (2015).
57. Chang, C.-C. & Lin, C.-J. LIBSVM: A library for support vector machines. *ACM Trans. Intell. Syst. Technol.* **2**, 27:1-27:27 (2011).

ED Fig. 1

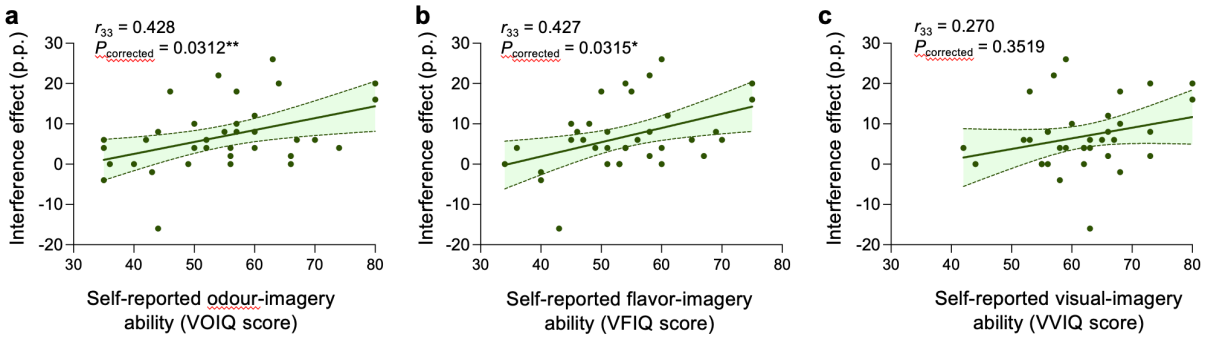
a
r_{33} = 0.428
$P_{corrected}$ = 0.0312**
Interference effect (p.p.)
Self-reported odour-imagery ability (VOIQ score)
b
r_{33} = 0.427
$P_{corrected}$ = 0.0315*
Interference effect (p.p.)
Self-reported flavor-imagery ability (VFIQ score)
c
r_{33} = 0.270
$P_{corrected}$ = 0.3519
Interference effect (p.p.)
Self-reported visual-imagery ability (VVIQ score)

ED Fig. 2

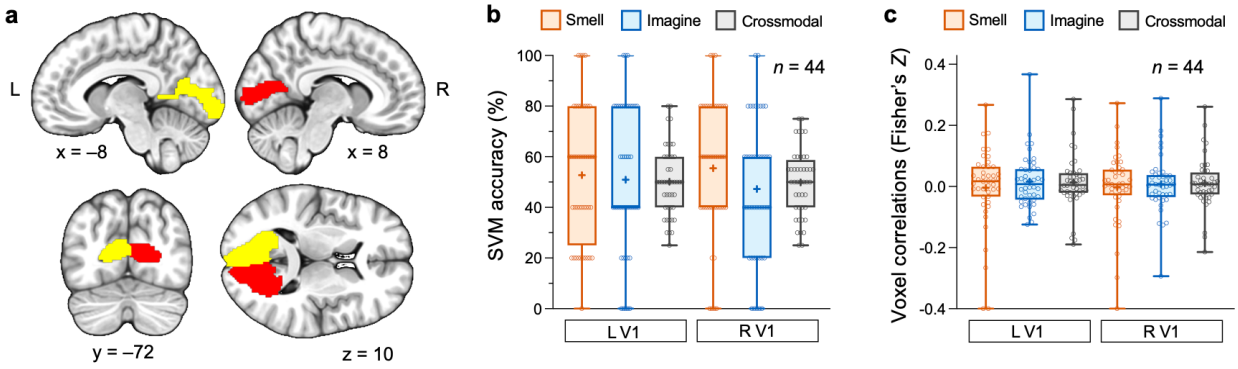
a
L
R
x = –8
x = 8
y = –72
z = 10
b
Smell
Imagine
Crossmodal
SVM accuracy (%)
100
80
60
40
20
0
n = 44
L V1
R V1
c
Smell
Imagine
Crossmodal
Voxel correlations (Fisher's Z)
0.4
0.2
0.0
-0.2
-0.4
n = 44
L V1
R V1

ED Fig. 3

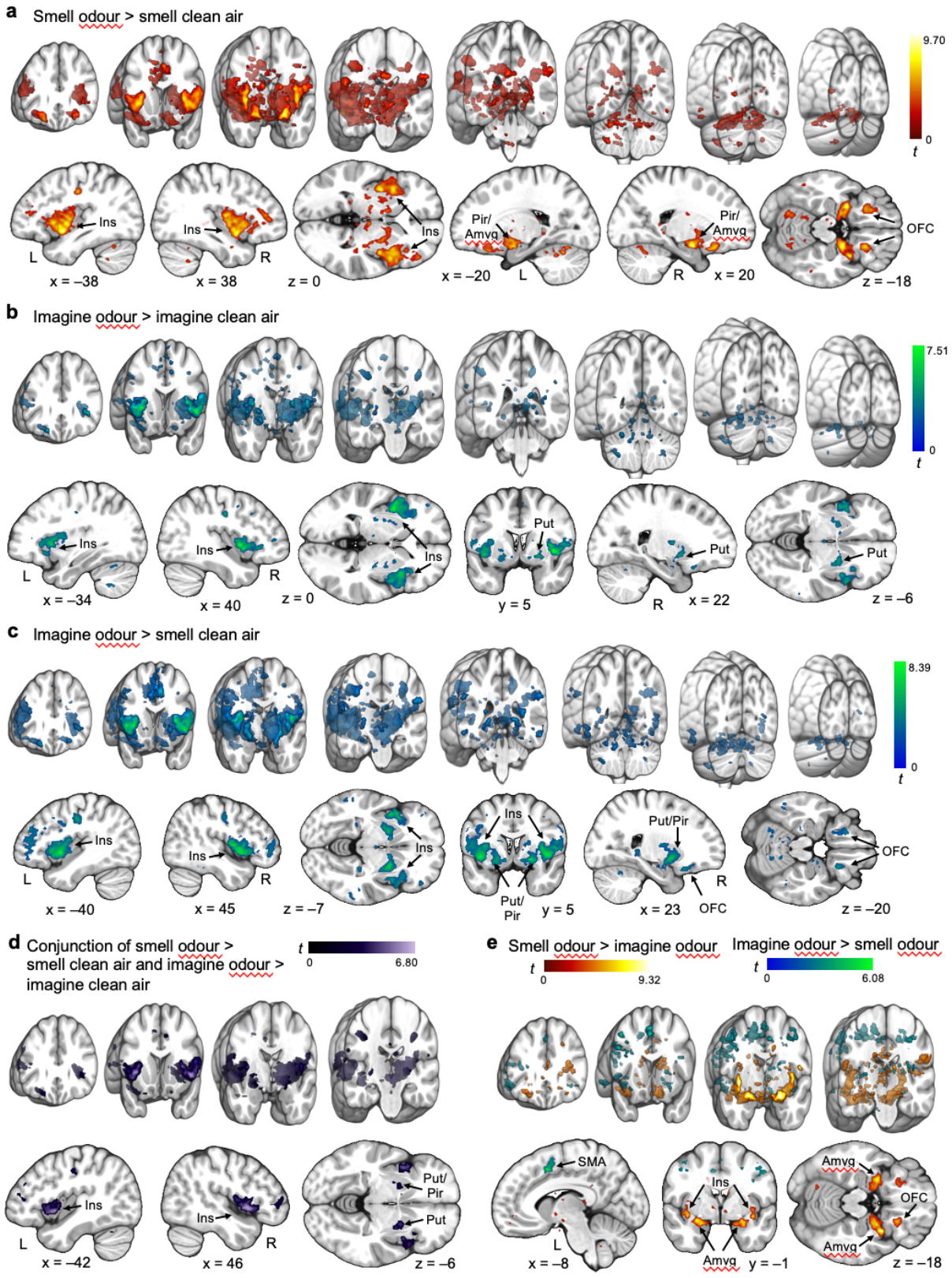
a
Smell odour > smell clean air
9.70
0
t
Ins
L
x = –38
Ins
R
x = 38
Ins
z = 0
Pir/
Amyg
x = –20
L
Pir/
Amyg
R
x = 20
OFC
z = –18
b
Imagine odour > imagine clean air
7.51
0
t
Ins
L
x = –34
Ins
R
x = 40
Ins
z = 0
Put
y = 5
Put
R
x = 22
Put
z = –6
c
Imagine odour > smell clean air
8.39
0
t
Ins
L
x = –40
Ins
R
x = 45
Ins
z = –7
Ins
Put/
Pir
y = 5
Put/Pir
R
x = 23
OFC
OFC
z = –20
d
Conjunction of smell odour > smell clean air and imagine odour > imagine clean air
t
0
6.80
Ins
L
x = –42
Ins
R
x = 46
Put/
Pir
Put
z = –6
e
Smell odour > imagine odour
t
0
9.32
Imagine odour > smell odour
t
0
6.08
SMA
L
x = –8
Ins
Amyg
y = –1
Amyg
OFC
Amyg
z = –18

ED Fig. 4

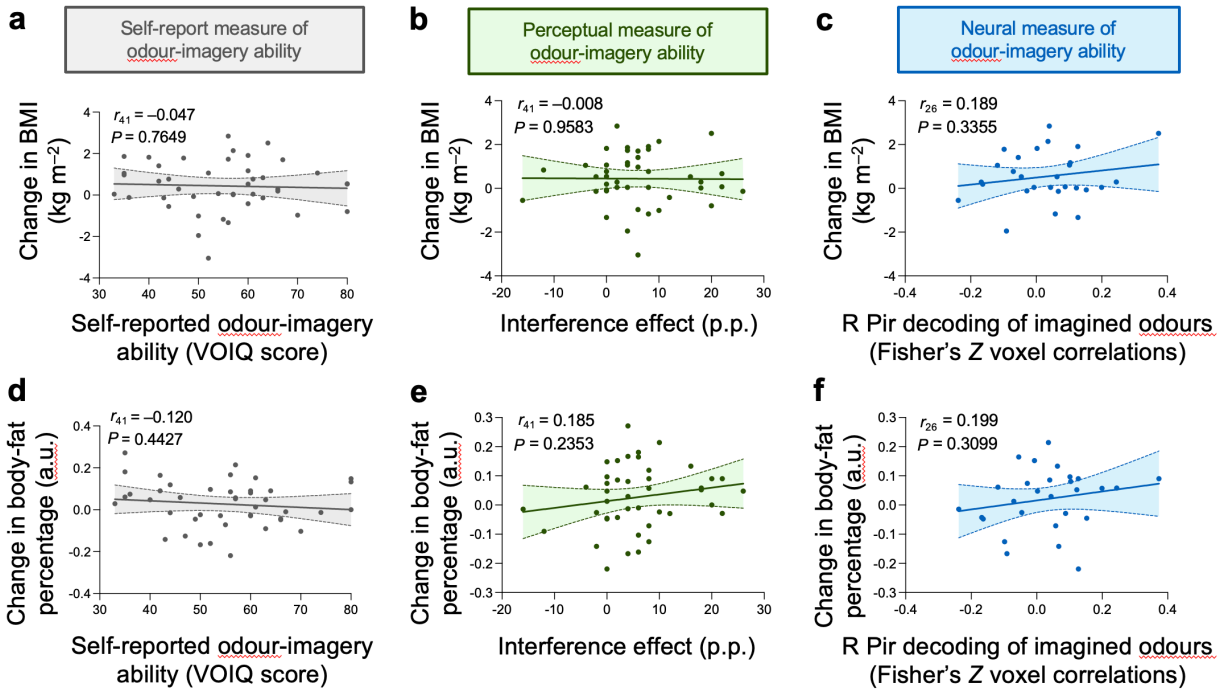
a
Self-report measure of odour-imagery ability
b
Perceptual measure of odour-imagery ability
c
Neural measure of odour-imagery ability
Change in BMI (kg m−2)
r41 = –0.047
P = 0.7649
r41 = –0.008
P = 0.9583
r26 = 0.189
P = 0.3355
Self-reported odour-imagery ability (VOIQ score)
Interference effect (p.p.)
R Pir decoding of imagined odours (Fisher's Z voxel correlations)
d
e
f
Change in body-fat percentage (a.u.)
r41 = –0.120
P = 0.4427
r41 = 0.185
P = 0.2353
r26 = 0.199
P = 0.3099
Self-reported odour-imagery ability (VOIQ score)
Interference effect (p.p.)
R Pir decoding of imagined odours (Fisher's Z voxel correlations)

ED Fig. 5

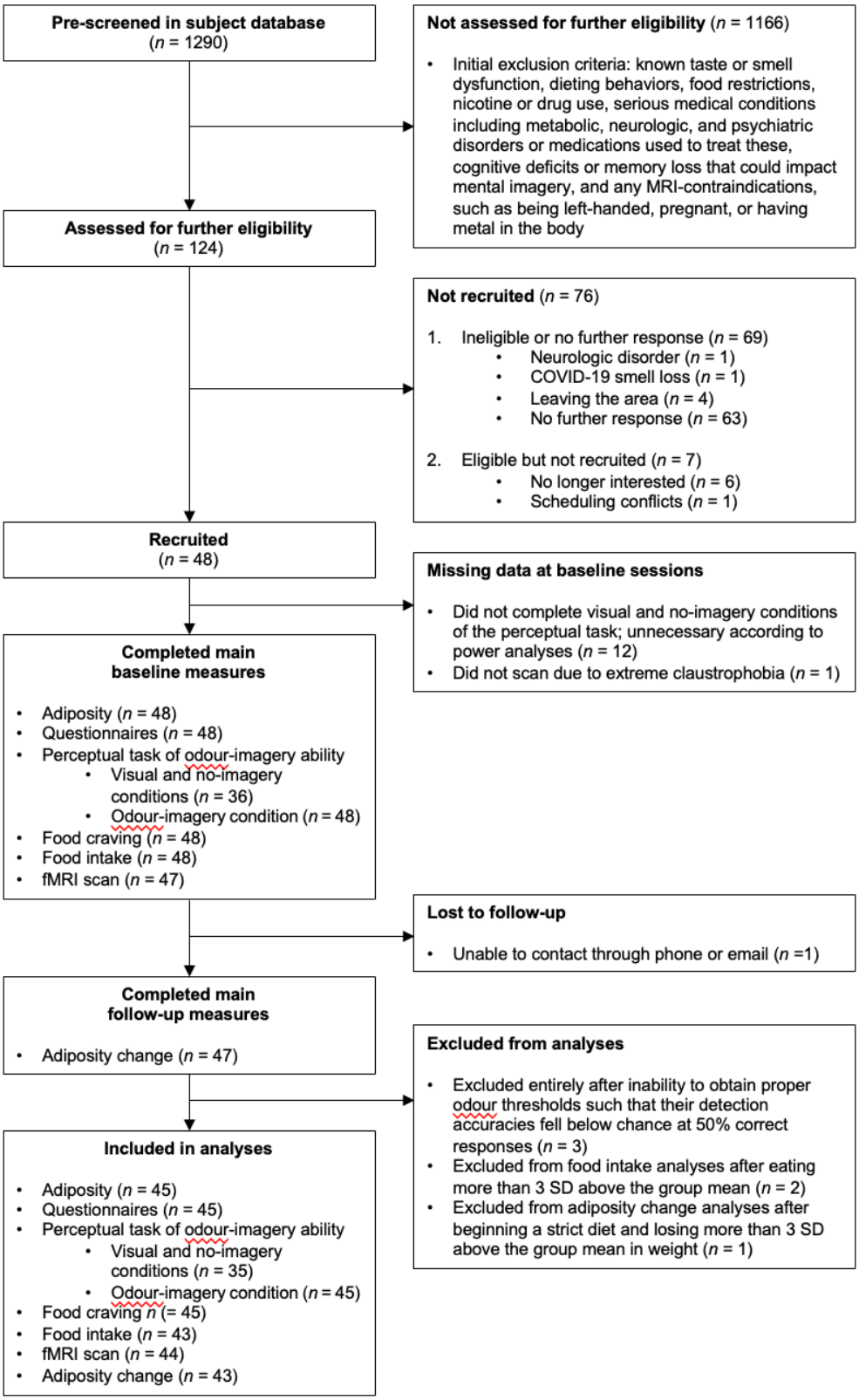
Pre-screened in subject database (n = 1290)
Not assessed for further eligibility (n = 1166)
• Initial exclusion criteria: known taste or smell dysfunction, dieting behaviors, food restrictions, nicotine or drug use, serious medical conditions including metabolic, neurologic, and psychiatric disorders or medications used to treat these, cognitive deficits or memory loss that could impact mental imagery, and any MRI-contraindications, such as being left-handed, pregnant, or having metal in the body
Assessed for further eligibility (n = 124)
Not recruited (n = 76)
1. Ineligible or no further response (n = 69)
• Neurologic disorder (n = 1)
• COVID-19 smell loss (n = 1)
• Leaving the area (n = 4)
• No further response (n = 63)
2. Eligible but not recruited (n = 7)
• No longer interested (n = 6)
• Scheduling conflicts (n = 1)
Recruited (n = 48)
Missing data at baseline sessions
• Did not complete visual and no-imagery conditions of the perceptual task; unnecessary according to power analyses (n = 12)
• Did not scan due to extreme claustrophobia (n = 1)
Completed main baseline measures
• Adiposity (n = 48)
• Questionnaires (n = 48)
• Perceptual task of odour-imagery ability
• Visual and no-imagery conditions (n = 36)
• Odour-imagery condition (n = 48)
• Food craving (n = 48)
• Food intake (n = 48)
• fMRI scan (n = 47)
Lost to follow-up
• Unable to contact through phone or email (n =1)
Completed main follow-up measures
• Adiposity change (n = 47)
Excluded from analyses
• Excluded entirely after inability to obtain proper odour thresholds such that their detection accuracies fell below chance at 50% correct responses (n = 3)
• Excluded from food intake analyses after eating more than 3 SD above the group mean (n = 2)
• Excluded from adiposity change analyses after beginning a strict diet and losing more than 3 SD above the group mean in weight (n = 1)
Included in analyses
• Adiposity (n = 45)
• Questionnaires (n = 45)
• Perceptual task of odour-imagery ability
• Visual and no-imagery conditions (n = 35)
• Odour-imagery condition (n = 45)
• Food craving n (= 45)
• Food intake (n = 43)
• fMRI scan (n = 44)
• Adiposity change (n = 43)

ED Fig. 6

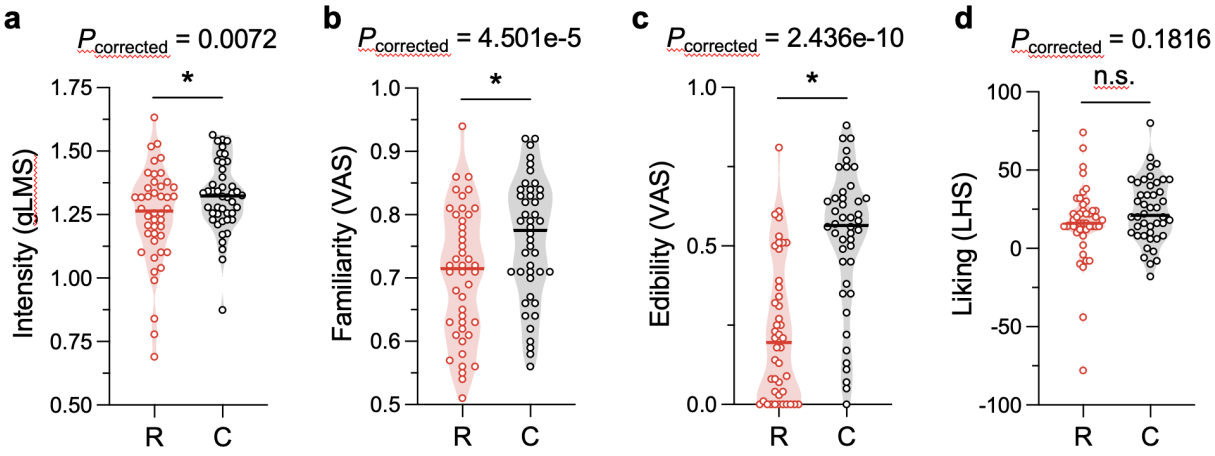
a
P corrected = 0.0072
*
Intensity (gLMS)
1.75
1.50
1.25
1.00
0.75
0.50
R
C
b
P corrected = 4.501e-5
*
Familiarity (VAS)
1.0
0.9
0.8
0.7
0.6
0.5
R
C
c
P corrected = 2.436e-10
*
Edibility (VAS)
1.0
0.5
0.0
R
C
d
P corrected = 0.1816
n.s.
Liking (LHS)
100
50
0
-50
-100
R
C

ED Fig. 7

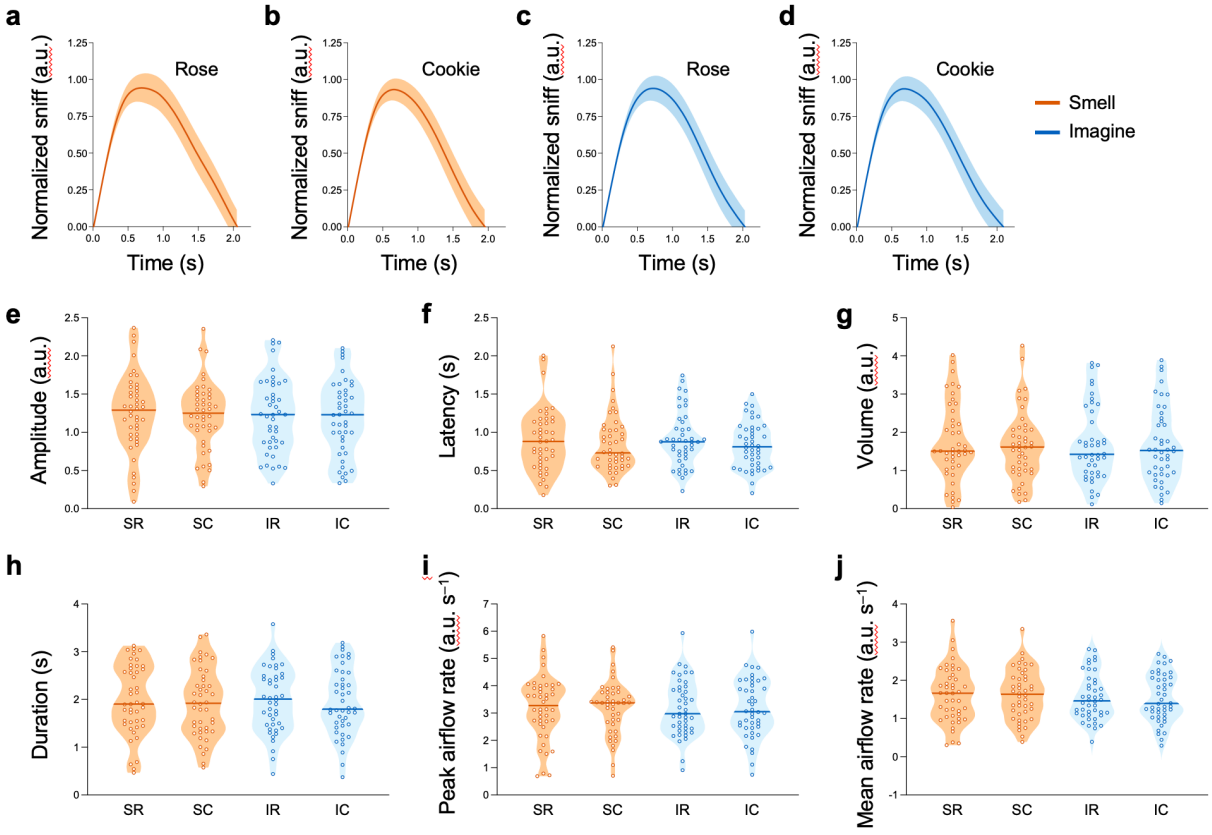
a
b
c
d
Rose
Cookie
Rose
Cookie
Normalized sniff (a.u.)
Time (s)
Smell
Imagine
e
f
g
h
i
j
Amplitude (a.u.)
Latency (s)
Volume (a.u.)
Duration (s)
Peak airflow rate (a.u. s^{-1})
Mean airflow rate (a.u. s^{-1})
SR
SC
IR
IC